Published in final edited form as:
Mol Cancer Ther. 2013 May ; 12(5): . doi:10.1158/1535-7163.MCT-12-1240.

Impact of Tumor Vascularity on Responsiveness to Anti-angiogenesis in a Prostate Cancer Stem Cell-derived Tumor Model

Kexiong Zhang and **David J. Waxman***
Division of Cell and Molecular Biology, Department of Biology, Boston University, 5 Cummington Street, Boston, MA 02215

Abstract

Drugs that target the tumor vasculature and inhibit angiogenesis are widely used for cancer treatment. Individual tumors show large differences in vascularity, but it is uncertain how these differences affect responsiveness to anti-angiogenesis. We investigated this question using two closely related prostate cancer models that differ markedly in tumor vascularity: PC3, which has very low vascularity, and the PC3-derived cancer stem-like cell holoclone PC3/2G7, which forms tumors with high microvessel density, high tumor blood flow and low hypoxia compared to parental PC3 tumors. Three angiogenesis inhibitors (axitinib, sorafenib, DC101) all induced significantly greater decreases in tumor blood flow and microvessel density in PC3/2G7 tumors compared to PC3 tumors, as well as significantly greater decreases in tumor cell proliferation and cell viability and a greater increase in apoptosis. The increased sensitivity of PC3/2G7 tumors to anti-angiogenesis indicates they are less tolerant of low vascularity and suggests they become addicted to their oxygen- and nutrient-rich environment. PC3/2G7 tumors showed strong up-regulation of the pro-angiogenic factors CCL2 and VEGFA compared to PC3 tumors, which may contribute to their increased vascularity, and they have significantly lower endothelial cell pericyte coverage, which may contribute to their greater sensitivity to anti-angiogenesis. Interestingly, high levels of VEGF receptor-2 were expressed on PC3 but not PC3/2G7 tumor cells, which may contribute to the growth static response of PC3 tumors to VEGF-targeted anti-angiogenesis. Finally, prolonged anti-angiogenic treatment led to resumption of PC3/2G7 tumor growth and neo-vascularization, indicating these cancer stem-like cell-derived tumors can adapt and escape from anti-angiogenesis.

Keywords

anti-angiogenesis; tumor vascularity; VEGF receptor

Introduction

Chemotherapy using cytotoxic drugs is presently the most commonly used weapon in the treatment of advanced cancer. However, the therapeutic efficacy of cancer chemotherapy is limited by factors such as tumor heterogeneity, host toxicity and drug resistance. New opportunities to improve cancer therapy are presented by drugs that target the tumor vasculature and inhibit tumor angiogenesis (1). Anti-angiogenesis may also help circumvent resistance to conventional chemotherapy linked to cancer stem cells (2, 3). Tumor

*Address correspondence to: Dr. David J. Waxman, Department of Biology, 5 Cummington Mall, Boston, MA 02215 USA, djw@bu.edu, Fax: 617-353-7404.

Disclosure of potential conflicts of Interest: The authors have no conflicts of interest to disclose.

angiogenesis is a highly regulated process, whereby new blood vessels form within growing tumors. In many cancers, as tumor cells proliferate, the tumor mass expands beyond the support capacity of the existing vasculature leading to decreased levels of oxygen and nutrients and the accumulation of metabolic wastes. Tumor cells respond to this deterioration of the microenvironment by secreting pro-angiogenic factors, which activate quiescent endothelial cells and promote their migration into the tumor. This shift of the tumor microenvironment to an angiogenic state, or “angiogenic switch” (4), is an important step in tumor development.

Inhibition of angiogenesis has emerged as an important therapeutic strategy for solid tumors. The VEGF pathway is the dominant signaling pathway involved in tumor angiogenesis (5), with VEGF receptor-2 (VEGFR2) being a major endothelial cell signal mediator and an important target of receptor tyrosine kinase inhibitors (RTKI) designed to inhibit tumor angiogenesis (5). Many tumor cells secrete VEGFA, which binds VEGF receptors on endothelial cells and stimulates vascular endothelial cell growth. VEGFA may also act as a direct tumor cell growth factor by binding VEGF receptors expressed on tumor cells (6, 7). Several anti-angiogenic drugs have been introduced in the clinic in the past few years, including the anti-VEGFA antibody bevacizumab and multi-receptor tyrosine kinase inhibitors (RTKIs), such as sorafenib and sunitinib (8). Greater selectivity for VEGFR inhibition can be achieved using the VEGFR2 monoclonal antibody DC101 (9, 10) or the RTKI axitinib, which preferentially inhibits VEGFR compared to other receptor tyrosine kinases (11). To date, however, the clinical benefits of these agents in unselected patient populations have been modest owing to factors such as increased invasiveness, decreased uptake of co-administered chemotherapeutics, and the development of tumor resistance (12–14).

Tumor vascularity has a major impact on tumor growth and drug responsiveness through its effects on tumor blood flow, oxygenation, and the permeability of chemotherapeutic drugs. Tumor vascularity varies widely in human cancers, ranging from highly vascularized renal carcinomas (15, 16) to poorly vascularized prostate cancer (17), reflecting, in part, the balance between pro- and anti-angiogenic factors within the tumor microenvironment (4, 18). Vascularity is an independent prognostic factor for many human tumors, with high vascular density often associated with poor prognosis following surgery or conventional chemo/radiotherapy (19, 20). For example, the progression of prostate cancer to androgen independence is characterized by increased angiogenesis, with increased vascular density associated with decreased survival (21). The vascularity of prostate cancer is in part dependent on VEGF (22, 23), with VEGF receptors being up regulated in metastatic prostate tumors (24). It is uncertain, however, whether high vascularity increases or decreases tumor responsiveness to anti-angiogenesis.

Well-vascularized tumors with elevated VEGF signaling (e.g., renal cell carcinoma) are considered to be a preferred target of anti-angiogenic drugs (25), whereas hypovascularized tumors are viewed as more hypoxia-tolerant and therefore likely to be less sensitive to anti-angiogenesis (26, 27). Changes in vascularity as a function of the stage of tumor growth and progression can impact the effectiveness of anti-angiogenic therapy, in part reflecting changes in vascular maturity, with blood vessels covered by pericytes and vascular smooth muscle cells more likely to survive anti-angiogenic drug treatment (28, 29). However, it is not clear whether the most highly vascularized tumors are necessarily the most responsive to anti-angiogenesis. Some studies found that slowly growing, poorly vascularized tumors respond to anti-angiogenic drug treatment as well as rapidly growing, highly vascularized tumors (30), while other studies reported increased responsiveness of poorly vascularized tumors (31, 32). Conceivably, anti-angiogenesis may suppress an already low blood supply to the point where continued tumor growth becomes unsustainable, in particular when

combined with chemotherapy (14). However, the limited data available on the impact of tumor vascularity on the efficacy of anti-angiogenic therapy are difficult to interpret, however, owing to intrinsic differences in the tumor models being compared, including differences in histology and tissue of origin, oncogenic mutation background, and VEGF-dependence of the tumor vasculature.

Presently, we investigate the impact of vascularity on anti-angiogenesis using two closely related prostate cancer tumor models that show marked differences in vascularity: parental PC3 prostate cancer tumors, which have very low vascularity (32), and PC3/2G7 tumors (33), which are grown from a cancer stem-like cell isolated from a PC3 parental cell population and are characterized by high vascularity. Further, we identify factors that may contribute to the increased vascularity of PC3/2G7 tumors, and we investigate the impact of long-term anti-angiogenesis in this cancer stem-like cell-derived tumor model. Our findings reveal a strong dependence of PC3/2G7 tumors on their high vascularity, and provide important new insight into the impact of tumor vascularity on responsiveness to anti-angiogenic drug treatment.

Materials and Methods

Chemicals and antibodies

Axitinib was obtained from Pfizer Global Research and Development (Pearl River, NY). Paraformaldehyde solution (16%; methanol-free) was purchased from Electron Microscopy Sciences (Hatfield, PA). Sorafenib was purchased from LC Laboratories (Woburn, MA). Mouse monoclonal antibody DC101 was kindly supplied by ImClone System (New York, NY). Normal rabbit serum, normal horse serum, avidin/biotin blocking kit, VECTASTAIN ABC Kit, peroxidase substrate VIP, DAB (3,3′-diaminobenzidine), TMB (3,3′,5,5′-tetramethylbenzidine), and VectaMount were purchased from Vector Laboratories (Burlingame, CA). Modified Mayer's hematoxylin (Cat. #S3301) was purchased from DAKO (Carpinteria, CA). DeadEnd Colorimetric terminal deoxynucleotidyltransferase-mediated dUTP nick end labeling (TUNEL) kit and RNase-free DNase (Cat. #M6101) were purchased from Promega (Madison, WI). RPMI 1640 culture medium, fetal bovine serum, and TRIzol were purchased from Invitrogen (Grand Island, NY). High capacity cDNA reverse transcription kit, random hexamers, MuLV reverse transcriptase, RNase inhibitor, and SYBR Green PCR Master Mix were purchased from Applied Biosystems (Carlsbad, CA).

Cell lines

PC3 human prostate cancer cells were authenticated by and obtained from Developmental Therapeutics Program (National Cancer Institute, Bethesda, MD) and were grown at 37°C in a humidified 5% CO_2 atmosphere in RPMI 1640 containing 7% fetal bovine serum. The PC3 stem cell-like clone PC3/2G7 was isolated from a population of PC3 cells as a holoclone; it was verified by spheroid formation assays and propagated as a cell line under conditions where it retains its cancer stem-like character (33). PC3/2G7 cells and parental PC3 cells were amplified using the same standard tissue culture conditions; cultures were split 1:3 when the cells reached 70–80% confluence. When passaged under these sub-confluent conditions, PC3/2G7 cells retained their holoclone-forming ability, as determined by replating the cells at 50–200 cells/cm^2 in a colony formation assay (33).

Tumor xenograft models

The effect of drug treatment on tumor growth was studied in PC3/2G7 and parent PC3 tumor xenografts grown in male scid immunodeficient mice (Fox Chase ICR-scid strain). Mice 5 to 7 wk old were purchased from Taconic Inc. (Germantown, NY) and housed in the

Boston University Laboratory of Animal Care Facility in accordance with institutionally approved protocols and federal guidelines. Autoclaved cages containing food and water were changed once a week. Mouse body weight was measured every 3 to 4 days. On the day of tumor cell inoculation, PC3/2G7 and parental PC3 tumor cells at 70 to 80% confluence were trypsinized and resuspended in serum-free culture medium. Tumor cells (4×10^6 cells in 0.2 ml) were implanted bilaterally by s.c. injection into each flank of the mouse. Tumor sizes were measured every 3 to 4 days using digital calipers (VWR International) and volumes were calculated as $V = (\pi/6) \times (L \times W)^{3/2}$. Mice were randomized to different treatment groups on the day of initial drug treatment, i.e., when the average tumor volume reached 400 to 600 mm^3 (10–14 tumors per treatment group). Mice were euthanized when they approached authorized tumor size limits specified in the approved animal protocol.

Anti-angiogenic drug treatment schedules and tumor growth delay experiments

Axitinib was administered to the tumor-bearing mice daily by i.p. injection at 25 mg/kg body weight and in a volume of 5 μl/g body weight. Control mice received daily i.p. injection of vehicle (30% polyethylene glycol 400/70% acidified water, pH 2–3) in a volume of 5 μl/g bodyweight. Axitinib was prepared as a 5 mg/ml suspension in 30% polyethylene glycol 400/70% acidified water, as follows. Axitinib (25 mg) was added to 1.5 ml of polyethylene glycol 400 and sonicated at room temperature for 10 to 20 min to obtain a fine suspension. The pH was adjusted to 2 to 3 using 0.1 N HCl followed by a second sonication. The volume was adjusted to 5 ml by adding acidified water (pH 2–3). The injection-ready solution was prepared fresh every 4 to 5 days and stored at 4°C in the dark. Sorafenib was administered by daily i.p. injection at 25 mg/kg mouse body weight. Weight appropriate volumes of sorafenib (6.25 μl per g body weight) were dissolved in sterile dimethylsulfoxide at 200 mg/ml and diluted in sterile 1× PBS (final concentration: 5.4 mg/ml of sorafenib tosylate (salt), which corresponds to 4 mg/ml of sorafenib). Fresh stock solutions of sorafenib were prepared every 6 days and stored in the dark at 4°C. Monoclonal antibody DC101 (10.86 mg/ml in PBS; Imclone lot#100726) was stored at 4°C and given by i.p. injection every 3 days at a dose of 28.6 mg/kg body weight (800 μg/28 g mouse) (34).

Hoechst 33342 perfusion assay

The DNA-binding dye Hoechst 33342 was used to analyze the patency of the tumor vasculature as described (32). Images were captured and analyzed using an Olympus FSX100 Bio Imaging Navigator fluorescence microscope system (Olympus America Inc., Center Valley, PA). Representative fields of the fluorescent staining patterns are presented for each tissue.

Immunohistochemistry and TUNEL staining

Tissues were cut to 6 μm as cryosections or paraffin-embedded sections. Immunohistochemical staining of cryosections was described previously (33). To prepare paraffin-embedded sections, tumor tissues pretreated with isopentane and stored at −80°C were fixed in 4% paraformaldehyde while the tissues thawed at room temperature. After 1 hr, the tissues were cooled to 4°C and shipped to Maine Health Center (Portland, ME) for preparation of paraffin-embedded blocks. Each tumor was cut into 3–4 pieces and embedded in the same block. Paraffin-embedded sections were baked, de-waxed and treated with 3% H_2O_2 for 10 min to inactivate endogenous peroxidases. Antigen retrieval was carried out by steaming in 10 mM citric buffer, pH 6 for 30 min. The samples were cooled to room temperature and then processed in an i6000 autostainer (Biogenex Inc., San Ramon, CA) as follows: 20 min serum blocking, 1 h primary antibody incubation, 1 h secondary antibody incubation, 30 min ABC incubation, and 5 min substrate incubation. IHC SuperSensitive buffer (Biogenex Inc.) was used for the intermediate wash steps. Following a thorough wash with tap water, the slides were dehydrated and sealed with VectaMount. The final dilution of

each primary antibody was as follows. For cryosections: anti-mouse CD31 (1:1000) (BD Pharmingen, San Diego, Cat. #557355) and anti-VEGFR2 (1:300) (Cell Signaling Technology, Danvers, MA, Cat. #2479); and for paraffin-embedded sections: anti-mouse CD31 (1:40) (HistoBioTec, Miami Beach, FL, Cat. #DIA-310), anti-PCNA (1:2000) (Cell Signaling Technology, Cat. #2586), anti-cleaved caspase-3-(Asp175) (1:2000) (Cell Signaling Technology, Cat. #9661), anti-CCL2 (1:20) (R&D Systems, Cat. #MAB2791), anti-VEGFA (1:100) (Santa Cruz Biotechnology, Santa Cruz, CA, Cat. #sc-152), anti-GLUT1 (1:400) (Millipore, Bedford, MA, Cat. #07-1401), and anti-human CD31 (1:50) (Leica Microsystems Newcastle Ltd, Newcastle upon Tyne, Cat. #NCL-CD31-1A10). Biotinylated anti-rat, anti-rabbit and anti-mouse secondary antibodies were diluted to 1:200 (Vector Laboratories, Cat. #BA4000, BA1000, and BA-2000, respectively).

Paraffin-embedded sections were dewaxed and rehydrated then incubated with hematoxylin for 5 min. Sections were washed with distilled water, and then incubated with Scott's tap water (Cat. #S5134, Sigma, St. Louis, MO) for 10 min, following by a dH_2O wash. Images were captured at 4.2× amplification on an Olympus FSX100 instrument and saved in high-resolution format. The staining intensity of each image was quantified using NIH ImageJ software. The stained area percentage was expressed as a mean value ± SE for each tumor, based on all images from the 3–4 independent tumor sections analyzed. Immunohistochemical double staining was detailed previously (35). For GLUT1 and CD31 double staining, paraffin-embedded sections were first stained with GLUT1 antibody (detection with DAB substrate) and then stained with CD31 antibody (detection with VIP substrate). Paraffin-embedded sections from 12 day axitinib treated PC3/2G7 and PC3 tumors and drug-free control tumors were processed for TUNEL assay using the manufacturer's protocol. TUNEL positive cells or areas were quantified using NIH ImageJ software.

Immunofluorescence double staining of microvessels and pericytes

Pericytes were identified using antibody to α-smooth muscle actin (α-SMA), which is expressed in several cell types but can be used to identify pericytes when used in combination with CD31 immunostaining to identify pericyte-associated vascular endothelial cells. Protocols and reagents purchased from Vector Laboratories were used. Briefly, 6 μm thick cryosections were cut from PC3/2G7 and PC3 tumor tissues, fixed in 1% paraformaldehyde for 30 min, then permeabilized with 1% Triton-X 100 (v/v) on ice. Slides were blocked with avidin/biotin and horse serum. The first staining was performed by incubating with anti-α-SMA antibody (1:400) for 45 min, followed by biotinylated anti-mouse antibody for 30 min, and then 15 μl/ml avidin-conjugated Fluorescein Avidin DCS (Cat. #A-1100, Vector Laboratories) for 10 min. The slides were reblocked with avidin/biotin and rabbit serum and incubated with anti-CD31 (1:1000) (BD Pharmingen) antibody for 1 hr followed by biotinylated anti-rat antibody for 30 min, and then 15 μl/ml avidin conjugated Texas Red Avidin DCS for 10 min. After a PBS wash, the slides were mounted and allowed to dry overnight. Images were captured with an Olympus FSX100 Bio Imaging Navigator fluorescence microscope using the green and red color emissions and the overlay function.

Real-time quantitative PCR (qPCR)

RNA levels were assayed in PC3/2G7 and PC3 tumors by qPCR using gene-specific, and in some cases species-specific, primer sequences shown in Supplemental Table 1. Fresh tumor tissue was snap-frozen in liquid nitrogen and stored at −80°C. Total RNA isolation, reverse transcription, and qPCR were performed as described elsewhere (33). C_T values determined for each RNA were normalized to the 18S rRNA content to give relative RNA levels.

Cell growth inhibition assay

The growth inhibitory effects of axitinib on cultured cells were investigated using a growth inhibition assay (36). Briefly, PC3/2G7, PC3 and 9L gliosarcoma cells were seeded in triplicate at 4×10^3 cells per well in 48-well plates and grown overnight. Cells were cultured for 4 days in the presence of axitinib (1 nM to 10 μM, final concentration), washed twice with PBS on ice, and then quantified by crystal violet staining at 595 nm. The staining intensity of drug-treated samples was calculated as a percentage of untreated controls based on triplicate assays.

Statistical analysis

Results were expressed as mean ± SE and are based on the indicated number of tumors or tissue samples per group. Statistical significance of differences was assessed by two-tailed Student's *t*-test or two-way ANOVA using GraphPad Prism software version 4.0; statistical significance is indicated by * $p < 0.05$, ** $p < 0.01$, and *** $p < 0.001$.

Results

High vascularity PC3/2G7 tumor model

PC3/2G7 is a clonal isolate from the human prostate cancer cell line PC3; it is one of several similar, independent clones derived from a sub-population of cancer stem-like cells present within the parental PC3 cell population and was isolated based on its characteristic holoclone morphology (33). Tumors derived from PC3/2G7 cells show significantly higher vascularity than parental PC3 cell-derived tumors, as indicated by immunostaining with anti-mouse CD31 antibody (Fig. 1A), and confirmed by the increased expression of CD31 and also VE-cadherin, a second marker of vascular endothelial cells (Fig. 1B, 1C). Tumor blood flow was substantially increased in PC3/2G7 tumors compared to PC3 tumors, as shown by Hoechst dye perfusion (Fig. 1D), indicating that the high-density PC3/2G7 blood vessels are functional. Immunostaining with anti-human CD31 was negative for both PC3 and PC3/2G7 tumors (c.f. normal human tonsil positive control; Supplemental Fig. 1). Thus, the dense blood vessels found in PC3/2G7 tumors are derived from host (mouse) endothelial cells and are not formed by differentiation of the (human) stem-like cells used to seed the PC3/2G7 tumors.

PC3/2G7 tumors are more responsive than PC3 tumors to axitinib anti-angiogenesis

Next, we investigated the responsiveness of PC3 and PC3/2G7 tumors to the VEGF receptor-selective angiogenesis inhibitor axitinib (11). Once established, PC3 and PC3/2G7 tumors grew at similar rates (Fig. 2A). Axitinib induced rapid onset of growth inhibition in both tumor models; however, whereas PC3 tumors continued to grow, albeit at a reduced rate, PC3/2G7 tumors began to regress after treatment day 6 (Fig. 2A). Furthermore, axitinib decreased tumor blood flow (Fig. 1D), resulting in a similar low level of vascularity in both tumor models after drug treatment (Fig. 2B, Supplemental Fig. 2A). Given the selectivity of axitinib for VEGF receptor inhibition *in vivo* (11), these findings indicate that the increased vascularity of PC3/2G7 tumors is VEGF receptor-dependent. Axitinib did not induce host toxicity in either tumor model, as judged by body weight measurements (data not shown).

Hematoxylin staining of tumor cell nuclei identifies viable tumor cells and distinguishes them from necrotic tumor regions that form after drug treatment, in a manner similar to YO-PRO-1 staining (37). Hematoxylin staining was significantly decreased in PC3/2G7 tumors but not PC3 tumors after 12 days axitinib treatment (Fig. 2C, Supplemental Fig. 2B). Moreover, tumor cell proliferation, monitored by PCNA staining, was significantly decreased by axitinib treatment of PC3/2G7 tumors but not PC3 tumors (Fig. 2D, Supplemental Fig. 2C). Axitinib also induced a significantly greater increase in apoptosis in

PC3/2G7 tumors than PC3 tumors, as revealed by TUNEL assay (Fig. 2E, Supplemental Fig. 2D). In cell culture, axitinib was not growth inhibitory to PC3/2G7 or PC3 cells, whereas it exhibited moderate growth-inhibitory activity against 9L tumor cells, which served as a positive control (36) (Supplemental Fig. 3). This suggests that the anti-tumor activities of axitinib seen *in vivo* (Fig. 2A) are indirect responses to the loss of VEGF signaling, and are not due to direct PC3/2G7 or PC3 tumor cell cytotoxicity.

Impact of sorafenib and DC101 on PC3/2G7 and PC3 tumors

Next, we investigated whether the greater sensitivity of PC3/2G7 tumors to axitinib is seen with two other anti-angiogenic drugs, the multi-RTKI sorafenib (38) and the anti-VEGFR2 monoclonal antibody DC101, which blocks VEGF-induced receptor activation (9, 10). With both drugs, PC3/2G7 tumor growth was inhibited more extensively and/or for a longer period of time than PC3 tumors (Supplemental Figs. 4 and 5). Blood flow to PC3/2G7 tumors was markedly decreased by both sorafenib and DC101, and a further decrease in the already low blood flow to PC3 tumors was also apparent (Fig. 3A). The treated PC3/2G7 tumors showed low microvessel density, with many blood vessels showing little internal volume in cross-sections, in contrast to the many large, open vessels found in untreated PC3/2G7 tumors (Fig. 3B). The few blood vessels detected in the sorafenib- and DC101-treated PC3 tumors were similar to or smaller than those in untreated PC3 tumors. The very low vascularity of the treated PC3/2G7 tumors was associated with more extensive tumor necrosis (fewer viable tumor regions), as indicated by lower hematoxylin staining (Fig. 3C), and a greater decrease in tumor cell proliferation (PCNA staining; Fig. 3D) compared to the drug-treated PC3 tumors. Thus, PC3/2G7 tumors are less able than PC3 tumors to tolerate the low vascularity induced by anti-angiogenesis.

Hypoxia, basal apoptosis and pericyte coverage

The tumor vasculature is characterized by structural and functional abnormalities that impart a tumor microenvironment marked by interstitial hypertension, hypoxia, and acidosis and impaired delivery of therapeutics (39). Immunostaining for GLUT-1, a well-established marker for tumor hypoxia, revealed more extensive hypoxic regions in PC3 tumors than in PC3/2G7 tumors (Fig. 4A), especially in tumor regions more distant from blood vessels (Fig. 4B). Further, apoptotic regions were more frequent in PC3 tumors than in PC3/2G7 tumors, as indicated by cleaved-caspase-3 immunostaining (Fig. 4C). The higher basal apoptotic rate in PC3 tumors is consistent with the increased apoptosis often seen in hypoxic tumors (27).

Pericytes wrap around endothelial cells and regulate blood vessel development and stabilization, and are recruited to tumor microvessels during angiogenesis (40). In contrast to normal tissue blood vessels, pericytes are loosely bounded to endothelial cells in tumor blood vessels, however, they still execute their functions, including secretion of survival signals and protection of vascular endothelial cells. We compared the pericyte coverage between PC3/2G7 tumors and PC3 tumors using α-SMA to stain pericytes, combined with CD31 staining to identify endothelial cells (Fig. 4D). Substantially fewer pericytes were found in PC3/2G7 tumors, despite their high vascular density, and correspondingly, the rate of pericyte coverage of tumor endothelial cells was much lower in PC3/2G7 tumors than in PC3 tumors (Fig. 4D, right; see overlap (yellow) between α-SMA and CD31).

Expression of pro-angiogenic factors in PC3/2G7 tumors

Next, we investigated factors that might contribute to the striking increase in vascularity seen in PC3/2G7 tumors. VEGFA protein levels were strongly up regulated in PC3/2G7 tumors compared to PC3 tumors (Fig. 5A), however, no differences in the expression of VEGFA RNA (Fig. 5B), VEGFC RNA (Supplemental Fig. 6A), or VEGFA splice variants

were apparent (data not shown). Large differences in expression of two other factors were seen: CCL2 (chemokine ligand 2, also termed MCP-1) was strongly up regulated and VEGFR2 was strongly down regulated in PC3/2G7 tumors compared to PC3 tumors, as shown by immunohistochemistry (Fig. 5A) and at the RNA level (Fig. 5B). CCL2 is an inflammatory chemokine that promotes angiogenesis, attracts tumor-promoting macrophages, and contributes to tumor progression and metastasis in many human cancers, including prostate cancer (41). The decreased expression of VEGFR2 in PC3/2G7 tumors might seem to be inconsistent with the increase in tumor angiogenesis and with the increased sensitivity of PC3/2G7 tumors to VEGF receptor-targeted anti-angiogenic drugs shown above. However, further analysis revealed that the decrease in overall PC3/2G7 tumor VEGFR2 levels reflects the all but complete repression of human (i.e., tumor cell-expressed) VEGFR2 (Fig. 5C, left). A similar loss of VEGFR2 expression was seen in PC3/2G7 tumor cells grown in culture (Fig. 5C, right). In contrast, PC3/2G7 tumor expression of mouse VEGFR2 (i.e., expression on tumor endothelial cells) was actually increased by ~2.5-fold compared to PC3 tumors (Fig. 5C, middle), consistent with the increased angiogenesis.

Escape from anti-angiogenesis

Despite the strong initial response of PC3/2G7 tumors to axitinib, PC3/2G7 tumors began to regrow after ~20 days daily axitinib treatment and continuing until day 58 (Fig. 6A), at which time the study was terminated due to the slow but steady decline in body weight associated with prolonged tumor burden combined with axitinib treatment (Fig. 6B). Tumor regrowth was associated with recovery of functional blood vessels, primarily at the tumor periphery, and this response contrasts to the marked overall decrease in tumor blood vessel density seen after the first 12 days axitinib treatment (Fig. 6C, 6D) (Supplemental Fig. 7). PC3/2G7 tumors treated with axitinib for 58 days showed an increase in proliferation (PCNA staining) when compared to tumors treated with axitinib for only 12 days (Fig. 6D), supporting the conclusion that these tumors escape from axitinib inhibition. Conceivably, this may occur by a VEGFR-independent angiogenic mechanism.

Discussion

The present study investigates the impact of tumor vascularity on responsiveness to anti-angiogenesis using two closely related prostate cancer tumor models, PC3 and the PC3 tumor stem-like cell-derived PC3/2G7 (33), which exhibits a growth rate very similar to PC3 but shows significantly higher vascularity. Our findings show that the more highly vascularized PC3/2G7 tumors are significantly more responsive to anti-angiogenesis, as determined using three different anti-angiogenic agents, axitinib, sorafenib (Fig. 7), and DC101. All three agents markedly reduced blood vessel density and dramatically decreased blood flow in PC3/2G7 tumors, whereas they induced much more modest changes in the poorly vascularized PC3 tumors. Importantly, PC3/2G7 tumor cell proliferation was inhibited more significantly by the anti-angiogenic drugs, and necrotic tumor regions and tumor cell apoptosis were more significantly increased as compared to PC3 tumors. Thus, anti-angiogenesis is more effective against PC3/2G7 tumors, whose increased sensitivity likely derives from the oxygen and/or nutrient starvation induced by anti-angiogenesis. In contrast, the anti-PC3 tumor responses to the angiogenesis inhibitors used here may be largely the result of direct inhibition of tumor cell-associated VEGF receptors, which are abundant on PC3 tumor cells, but are barely detectable on PC3/2G7 tumor cells (Fig. 5B), and presumably act as tumor growth factor receptors (6, 7). Notably, following anti-angiogenesis, tumor blood flow and microvessel density were as low in PC3/2G7 tumors as in PC3 tumors, yet the PC3/2G7 tumors showed significantly greater tumor cell apoptosis, more extensive necrotic regions, and lower tumor cell proliferation than PC3 tumors. These

findings support the conclusion that the PC3/2G7 tumors are less tolerant to low vascularity than PC3 tumors.

All tumors, including those of low microvessel density, depend on a therapeutically targetable angiogenic process driven by a requirement of nutrients and oxygen exchange for tumor growth. However, vascularity requirements differ significantly between tumors, and rapid tumor growth does not necessarily indicate high vascular density (18). Moreover, the microvessel density of a tumor is often lower than that of nearby normal tissue, which experiences no net growth (17). This difference may reflect the lower rate of oxygen consumption by tumor cells, which can tolerate oxygen deprivation and be resistant to apoptosis under hypoxic conditions (27). Consequently, the degree of tumor vascularity may be regarded as reflecting the metabolic burden of the supported tumor cells. Tumors that have high rates of oxygen or nutrient consumption, such as glioblastomas, often have high vascularity, whereas, tumors with a low metabolic demand, such as chondrosarcomas, are poorly vascularized (18). Thus, the high vascularity of PC3/2G7 tumors may indicate a higher metabolic rate compared to PC3 tumors. Importantly, we found that PC3/2G7 tumors are particularly sensitive to the loss of vasculature and decrease in tumor blood flow induced by anti-angiogenic drugs, whereas PC3 tumors readily tolerate these conditions. Highly vascularized tumors, such as PC3/2G7, may be good targets for clinical anti-angiogenic therapy.

PC3/2G7 endothelial cells were found to have a significantly lower rate of pericyte coverage than PC3 endothelial cells, as shown by double immunostaining of microvessels and pericyte cells. Pericytes wrap around vascular endothelial cells and provide them with survival signals essential for the stabilization and maintenance of mature blood vessels (28). The low rate of pericyte coverage in PC3/2G7 tumors compared to PC3 tumors is indicative of a more immature vascular system, and may contribute to the greater anti-angiogenic response of the PC3/2G7 tumors.

Prolonged treatment of PC3/2G7 tumors with axitinib led to an apparent escape from anti-angiogenesis, marked by neo-vascularization and the resumption of tumor growth. Several mechanisms may contribute to escape from VEGF receptor-targeted anti-angiogenesis. Tumor angiogenesis can become VEGF independent by up regulating alternative pro-angiogenic molecules that compensate for the loss of VEGF signaling. This may, in part, be facilitated by hypoxia induced by tumor vessel pruning, which induces factors that stimulate tumor vascularization (42). Therapy-induced hypoxia also plays a critical role in facilitating the selection of tumor cells that are able to tolerate, and perhaps even thrive, in a low oxygen environment (43).

We determined that the vasculature of human PC3/2G7 (and PC3) tumors is derived from host (mouse) vascular endothelial cells and does not contain detectable levels of human blood vessels, which, in principle, could form by differentiation of the (human) tumor stem-like cells used to seed the PC3/2G7 tumors. In contrast, tumor xenografts grown from human glioblastoma neurospheres develop human blood vessels (identified using human CD31-specific antibody), indicating that brain cancer stem-like cells can differentiate into functional tumor endothelial cells (44, 45). Using the same anti-human CD31 antibody, we observed strong positive staining of human normal tissues, whereas human CD31 staining of PC3/2G7 tumor blood vessels was undetectable. The same PC3/2G7 tumors showed strong staining by anti-mouse CD31 antibody, indicating that the majority of PC3/2G7 tumor blood vessels are of host (mouse) origin. The ability of brain tumor stem cells, but apparently not other tumor stem-like cells, to differentiate into tumor endothelial cells (44, 45) is consistent with reports that normal neuronal stem cells can differentiate into endothelial cells (46), and suggests that this differentiation pathway may be tissue type-dependent. In contrast, our

finding that VEGFA and CCL2 are up regulated in PC3/2G7 tumors compared to parental PC3 tumors is similar to the finding in other studies that brain cancer stem-like cells secret pro-angiogenic factors, which in turn recruit host endothelial cells to grow into tumor blood vessels (47, 48). The pro-angiogenic chemokine IL8 is another key determinant of prostate cancer vascularity; it is elevated in metastatic prostate cancer and stimulates angiogenesis and increases vascularity in many cancer types, including prostate tumors (49, 50), but was, in fact, decreased in PC3/2G7 tumors (Supplemental Fig. 6B). Further study is required to elucidate the full range of factors and mechanisms that lead to the increased angiogenesis of PC3/2G7 tumors.

In conclusion, we show, using the high vascularity, stem-like cell-derived prostate cancer model PC3/2G7 and its low vascularity PC3 parental tumor control, that highly vascularized tumors are more responsive to anti-angiogenesis and less tolerant of the loss of vascularity than poorly vascularized tumors. Thus, the vascularity status of tumors in individual patients – or perhaps levels of CCL2 or another associated pro-angiogenic marker up regulated in PC3/2G7 tumors – could be an important prognostic indicator of intrinsic susceptibility to anti-angiogenic therapies. Further studies are needed to establish whether the strong up-regulation of CCL2 and other pro-angiogenic factors drives the increased vascularity of PC3/2G7 tumors, and to ascertain whether these factors also determine the low pericyte coverage of PC3/2G7 tumor endothelial cells, which may contribute to the observed increase in sensitivity to anti-angiogenesis. Our finding that VEGFR2 was expressed at a high level on PC3 (but not PC3/2G7) tumor cells suggests VEGFR2 functions as a PC3 growth factor receptor, whose inhibition contributes to the PC3 tumor growth response seen with all three VEGF pathway-targeted drugs. Finally, PC3/2G7 tumors retained the ability to adapt and escape from anti-angiogenesis, as evidenced by the resumption of tumor growth and neo-vascularization following prolonged anti-angiogenic drug treatment, highlighting the need for more effective therapeutic approaches to such cancer stem-like cell-derived tumors.

Supplementary Material

Refer to Web version on PubMed Central for supplementary material.

Acknowledgments

We thank C.S. Chen, Dr. J. Connerney and Dr. L. Jia for assistance and many useful discussions.

Supported in part by NIH grant CA49248 (to D.J. Waxman)

References

1. Johannessen TC, Wagner M, Straume O, Bjerkvig R, Eikesdal HP. Tumor vasculature: the Achilles' heel of cancer? Expert Opin Ther Targets. 2013; 17:7–20. [PubMed: 23121690]
2. Eyler CE, Rich JN. Survival of the fittest: cancer stem cells in therapeutic resistance and angiogenesis. J Clin Oncol. 2008; 26:2839–45. [PubMed: 18539962]
3. Tang C, Ang BT, Pervaiz S. Cancer stem cell: target for anti-cancer therapy. FASEB J. 2007; 21:3777–85. [PubMed: 17625071]
4. Hanahan D, Folkman J. Patterns and emerging mechanisms of the angiogenic switch during tumorigenesis. Cell. 1996; 86:353–64. [PubMed: 8756718]
5. Tie J, Desai J. Antiangiogenic therapies targeting the vascular endothelia growth factor signaling system. Crit Rev Oncog. 2012; 17:51–67. [PubMed: 22471664]
6. Epstein RJ. VEGF signaling inhibitors: more pro-apoptotic than anti-angiogenic. Cancer Metastasis Rev. 2007; 26:443–52. [PubMed: 17786538]

7. Masood R, Cai J, Zheng T, Smith DL, Hinton DR, Gill PS. Vascular endothelial growth factor (VEGF) is an autocrine growth factor for VEGF receptor-positive human tumors. Blood. 2001; 98:1904–13. [PubMed: 11535528]
8. Cao Y. Tumor angiogenesis and molecular targets for therapy. Front Biosci. 2009; 14:3962–73.
9. Franco M, Man S, Chen L, Emmenegger U, Shaked Y, Cheung AM, et al. Targeted anti-vascular endothelial growth factor receptor-2 therapy leads to short-term and long-term impairment of vascular function and increase in tumor hypoxia. Cancer Res. 2006; 66:3639–48. [PubMed: 16585189]
10. Sweeney P, Karashima T, Kim SJ, Kedar D, Mian B, Huang S, et al. Anti-vascular endothelial growth factor receptor 2 antibody reduces tumorigenicity and metastasis in orthotopic prostate cancer xenografts via induction of endothelial cell apoptosis and reduction of endothelial cell matrix metalloproteinase type 9 production. Clinical cancer research : an official journal of the American Association for Cancer Research. 2002; 8:2714–24. [PubMed: 12171905]
11. Hu-Lowe DD, Zou HY, Grazzini ML, Hallin ME, Wickman GR, Amundson K, et al. Nonclinical antiangiogenesis and antitumor activities of axitinib (AG-013736), an oral, potent, and selective inhibitor of vascular endothelial growth factor receptor tyrosine kinases 1, 2, 3. Clin Cancer Res. 2008; 14:7272–83. [PubMed: 19010843]
12. Shojaei F. Anti-angiogenesis therapy in cancer: current challenges and future perspectives. Cancer Lett. 2012; 320:130–7. [PubMed: 22425960]
13. Young RJ, Reed MW. Anti-angiogenic therapy: concept to clinic. Microcirculation. 2012; 19:115–25. [PubMed: 22078005]
14. Ma J, Waxman DJ. Combination of antiangiogenesis with chemotherapy for more effective cancer treatment. Mol Cancer Ther. 2008; 7:3670–84. [PubMed: 19074844]
15. Sawhney R, Kabbinavar F. Angiogenesis and angiogenic inhibitors in renal cell carcinoma. Current urology reports. 2008; 9:26–33. [PubMed: 18366971]
16. Sciarra A, Gentile V, Salciccia S, Alfarone A, Di Silverio F. New anti-angiogenic targeted therapy in advanced renal cell carcinoma (RCC): current status and future prospects. Reviews on recent clinical trials. 2008; 3:97–103. [PubMed: 18474019]
17. Eberhard A, Kahlert S, Goede V, Hemmerlein B, Plate KH, Augustin HG. Heterogeneity of angiogenesis and blood vessel maturation in human tumors: implications for antiangiogenic tumor therapies. Cancer Res. 2000; 60:1388–93. [PubMed: 10728704]
18. Hlatky L, Hahnfeldt P, Folkman J. Clinical application of antiangiogenic therapy: microvessel density, what it does and doesn't tell us. J Natl Cancer Inst. 2002; 94:883–93. [PubMed: 12072542]
19. Sharma S, Sharma MC, Sarkar C. Morphology of angiogenesis in human cancer: a conceptual overview, histoprognostic perspective and significance of neoangiogenesis. Histopathology. 2005; 46:481–9. [PubMed: 15842629]
20. Hasan J, Byers R, Jayson GC. Intra-tumoural microvessel density in human solid tumours. British journal of cancer. 2002; 86:1566–77. [PubMed: 12085206]
21. Lissbrant IF, Stattin P, Damber JE, Bergh A. Vascular density is a predictor of cancer-specific survival in prostatic carcinoma. The Prostate. 1997; 33:38–45. [PubMed: 9294625]
22. Stefanou D, Batistatou A, Kamina S, Arkoumani E, Papachristou DJ, Agnantis NJ. Expression of vascular endothelial growth factor (VEGF) and association with microvessel density in benign prostatic hyperplasia and prostate cancer. In vivo (Athens, Greece). 2004; 18:155–60.
23. Donohue JF, Hayne D, Karnik U, Thomas DR, Foster MC. Randomized, placebo-controlled trial showing that finasteride reduces prostatic vascularity rapidly within 2 weeks. BJU international. 2005; 96:1319–22. [PubMed: 16287453]
24. Balbay MD, Pettaway CA, Kuniyasu H, Inoue K, Ramirez E, Li E, et al. Highly metastatic human prostate cancer growing within the prostate of athymic mice overexpresses vascular endothelial growth factor. Clin Cancer Res. 1999; 5:783–9. [PubMed: 10213213]
25. Negrier S, Raymond E. Antiangiogenic treatments and mechanisms of action in renal cell carcinoma. Invest New Drugs. 2012; 30:1791–801. [PubMed: 21573959]
26. Blagosklonny MV. Antiangiogenic therapy and tumor progression. Cancer Cell. 2004; 5:13–7. [PubMed: 14749122]

27. Graeber TG, Osmanian C, Jacks T, Housman DE, Koch CJ, Lowe SW, et al. Hypoxia-mediated selection of cells with diminished apoptotic potential in solid tumours. Nature. 1996; 379:88–91. [PubMed: 8538748]
28. Helfrich I, Schadendorf D. Blood vessel maturation, vascular phenotype and angiogenic potential in malignant melanoma: one step forward for overcoming anti-angiogenic drug resistance? Mol Oncol. 2011; 5:137–49. [PubMed: 21345752]
29. Benjamin LE, Golijanin D, Itin A, Pode D, Keshet E. Selective ablation of immature blood vessels in established human tumors follows vascular endothelial growth factor withdrawal. The Journal of clinical investigation. 1999; 103:159–65. [PubMed: 9916127]
30. Beecken WD, Fernandez A, Joussen AM, Achilles EG, Flynn E, Lo KM, et al. Effect of antiangiogenic therapy on slowly growing, poorly vascularized tumors in mice. J Natl Cancer Inst. 2001; 93:382–7. [PubMed: 11238700]
31. Fenton BM, Paoni SF, Grimwood BG, Ding I. Disparate effects of endostatin on tumor vascular perfusion and hypoxia in two murine mammary carcinomas. International journal of radiation oncology, biology, physics. 2003; 57:1038–46.
32. Ma J, Waxman DJ. Dominant effect of antiangiogenesis in combination therapy involving cyclophosphamide and axitinib. Clin Cancer Res. 2009; 15:578–88. [PubMed: 19147763]
33. Zhang K, Waxman DJ. PC3 prostate tumor-initiating cells with molecular profile FAM65Bhigh/MFI2low/LEF1low increase tumor angiogenesis. Mol Cancer. 2010; 9:319. [PubMed: 21190562]
34. Bocci G, Man S, Green SK, Francia G, Ebos JM, du Manoir JM, et al. Increased plasma vascular endothelial growth factor (VEGF) as a surrogate marker for optimal therapeutic dosing of VEGF receptor-2 monoclonal antibodies. Cancer Res. 2004; 64:6616–25. [PubMed: 15374976]
35. Ma J, Waxman DJ. Collaboration between hepatic and intratumoral prodrug activation in a P450 prodrug-activation gene therapy model for cancer treatment. Mol Cancer Ther. 2007; 6:2879–90. [PubMed: 17989319]
36. Ma J, Waxman DJ. Modulation of the antitumor activity of metronomic cyclophosphamide by the angiogenesis inhibitor axitinib. Mol Cancer Ther. 2008; 7:79–89. [PubMed: 18202011]
37. Hashizume H, Falcon BL, Kuroda T, Baluk P, Coxon A, Yu D, et al. Complementary actions of inhibitors of angiopoietin-2 and VEGF on tumor angiogenesis and growth. Cancer Res. 2010; 70:2213–23. [PubMed: 20197469]
38. Wilhelm SM, Adnane L, Newell P, Villanueva A, Llovet JM, Lynch M. Preclinical overview of sorafenib, a multikinase inhibitor that targets both Raf and VEGF and PDGF receptor tyrosine kinase signaling. Mol Cancer Ther. 2008; 7:3129–40. [PubMed: 18852116]
39. Carmeliet P, Jain RK. Principles and mechanisms of vessel normalization for cancer and other angiogenic diseases. Nat Rev Drug Discov. 2011; 10:417–27. [PubMed: 21629292]
40. Ribatti D, Nico B, Crivellato E. The role of pericytes in angiogenesis. Int J Dev Biol. 2011; 55:261–8. [PubMed: 21710434]
41. Zhang J, Patel L, Pienta KJ. CC chemokine ligand 2 (CCL2) promotes prostate cancer tumorigenesis and metastasis. Cytokine Growth Factor Rev. 2010; 21:41–8. [PubMed: 20005149]
42. Bergers G, Hanahan D. Modes of resistance to anti-angiogenic therapy. Nat Rev Cancer. 2008; 8:592–603. [PubMed: 18650835]
43. Hirota K, Semenza GL. Regulation of angiogenesis by hypoxia-inducible factor 1. Crit Rev Oncol Hematol. 2006; 59:15–26. [PubMed: 16716598]
44. Ricci-Vitiani L, Pallini R, Biffoni M, Todaro M, Invernici G, Cenci T, et al. Tumour vascularization via endothelial differentiation of glioblastoma stem-like cells. Nature. 2010; 468:824–8. [PubMed: 21102434]
45. Wang R, Chadalavada K, Wilshire J, Kowalik U, Hovinga KE, Geber A, et al. Glioblastoma stem-like cells give rise to tumour endothelium. Nature. 2010; 468:829–33. [PubMed: 21102433]
46. Wurmser AE, Nakashima K, Summers RG, Toni N, D'Amour KA, Lie DC, et al. Cell fusion-independent differentiation of neural stem cells to the endothelial lineage. Nature. 2004; 430:350–6. [PubMed: 15254537]
47. Bao S, Wu Q, Sathornsumetee S, Hao Y, Li Z, Hjelmeland AB, et al. Stem cell-like glioma cells promote tumor angiogenesis through vascular endothelial growth factor. Cancer Res. 2006; 66:7843–8. [PubMed: 16912155]

48. Folkins C, Shaked Y, Man S, Tang T, Lee CR, Zhu Z, et al. Glioma tumor stem-like cells promote tumor angiogenesis and vasculogenesis via vascular endothelial growth factor and stromal-derived factor 1. Cancer Res. 2009; 69:7243–51. [PubMed: 19738068]

49. Bao BY, Yao J, Lee YF. 1alpha, 25-dihydroxyvitamin D3 suppresses interleukin-8-mediated prostate cancer cell angiogenesis. Carcinogenesis. 2006; 27:1883–93. [PubMed: 16624828]

50. Kim SJ, Uehara H, Karashima T, McCarty M, Shih N, Fidler IJ. Expression of interleukin-8 correlates with angiogenesis, tumorigenicity, and metastasis of human prostate cancer cells implanted orthotopically in nude mice. Neoplasia (New York, NY. 2001; 3:33–42.

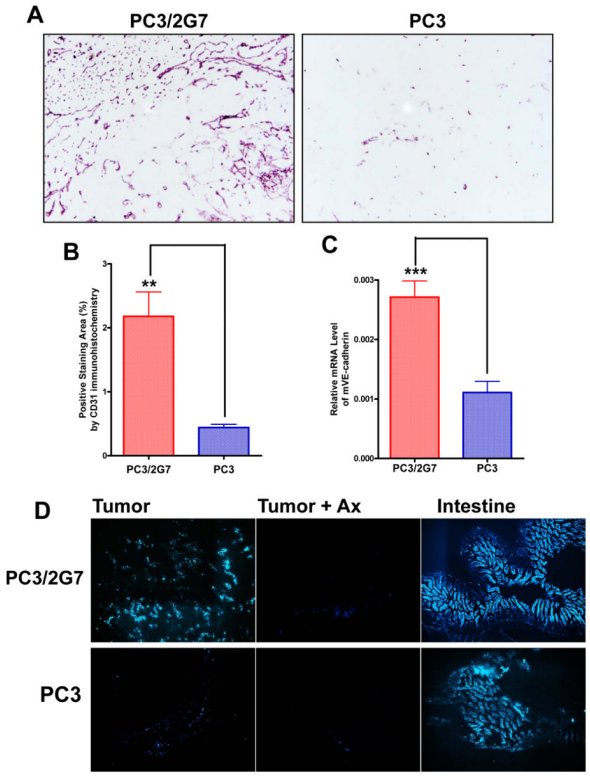

Figure 1. Vascularity of PC3/2G7 and PC3 tumor models

A. Representative CD31 immunostained cryosections of PC3/2G7 and PC3 tumors showing high and low microvessel density, respectively (magnification, 10x). **B**. Quantification of CD31 immunostained PC3/2G7 and PC3 tumors (as in A) using NIH ImageJ software. Data are mean ± SE values based on stained cryosections from three different regions of n=7 PC3/2G7 tumors and n=6 PC3 tumors; **, p=0.0015, for vascular area of PC3/2G7 vs. PC3 (two-tailed student's test). **C**. qPCR analysis of mouse endothelial cell marker VE-cadherin RNA levels. Shown are relative RNA levels based on n=10 PC3/2G7 tumors and n=12 PC3 tumors, mean ± SE; ***, p<0.0001, for PC3/2G7 vs. PC3 tumors, two-tailed student's test. **D**. Functional blood vessels in PC3/2G7 and PC3 tumor cryosections (magnification, 4.2×) assessed by Hoechst 33342 perfusion. Shown are fluorescence microscopic images of PC3/2G7 and PC3 tumors and intestines (normal tissue positive control) after 12 days axitinib treatment, as indicated ('Ax') from mice killed 1 min after Hoechst 33342 injection.

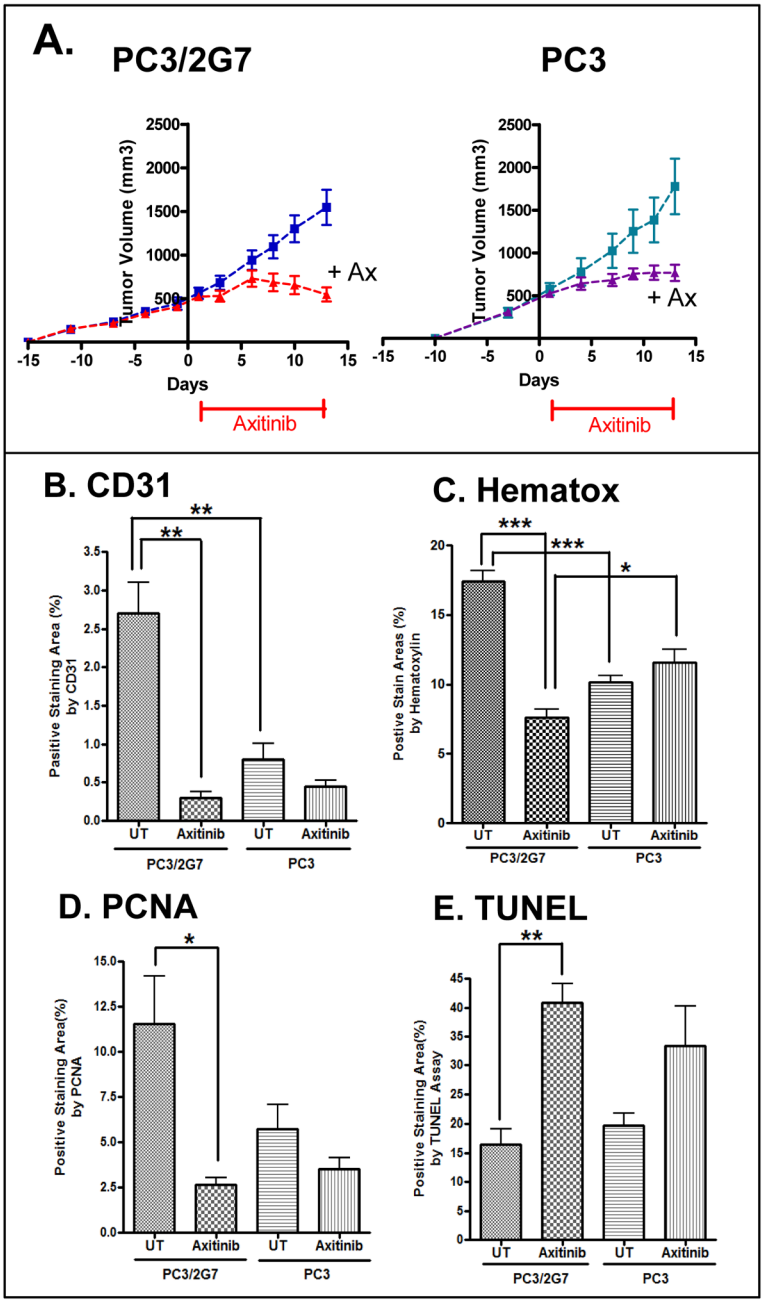

Figure 2. Anti-tumor activity of axitinib against PC3/2G7 and PC3 tumors

A. Effect of daily axitininb treatment (days 1–12) on tumor growth in male scid mice. Tumor volumes, mean ± SE, for n=10–14 tumor/group. **B–E,** Quantitative analysis of the effects of axitinib on: **B**, tumor microvessel density (CD31 staining); **C**, tumor cellularity (hematoxylin staining); **D**, tumor cell proliferation (PCNA staining); and **E**, apoptosis (TUNEL). Quantitation was determined using ImageJ. Data are mean ± SE values based on stained cryosections (magnification, 4.2×) from three different regions of n = 4 tumors/group. Representative stained images are shown in Supplemental Fig. 2. * $p<0.05$, ** $p<0.01$, *** $p<0.001$ by two-way ANOVA (A), or by two-tailed student's t-test (B–E).

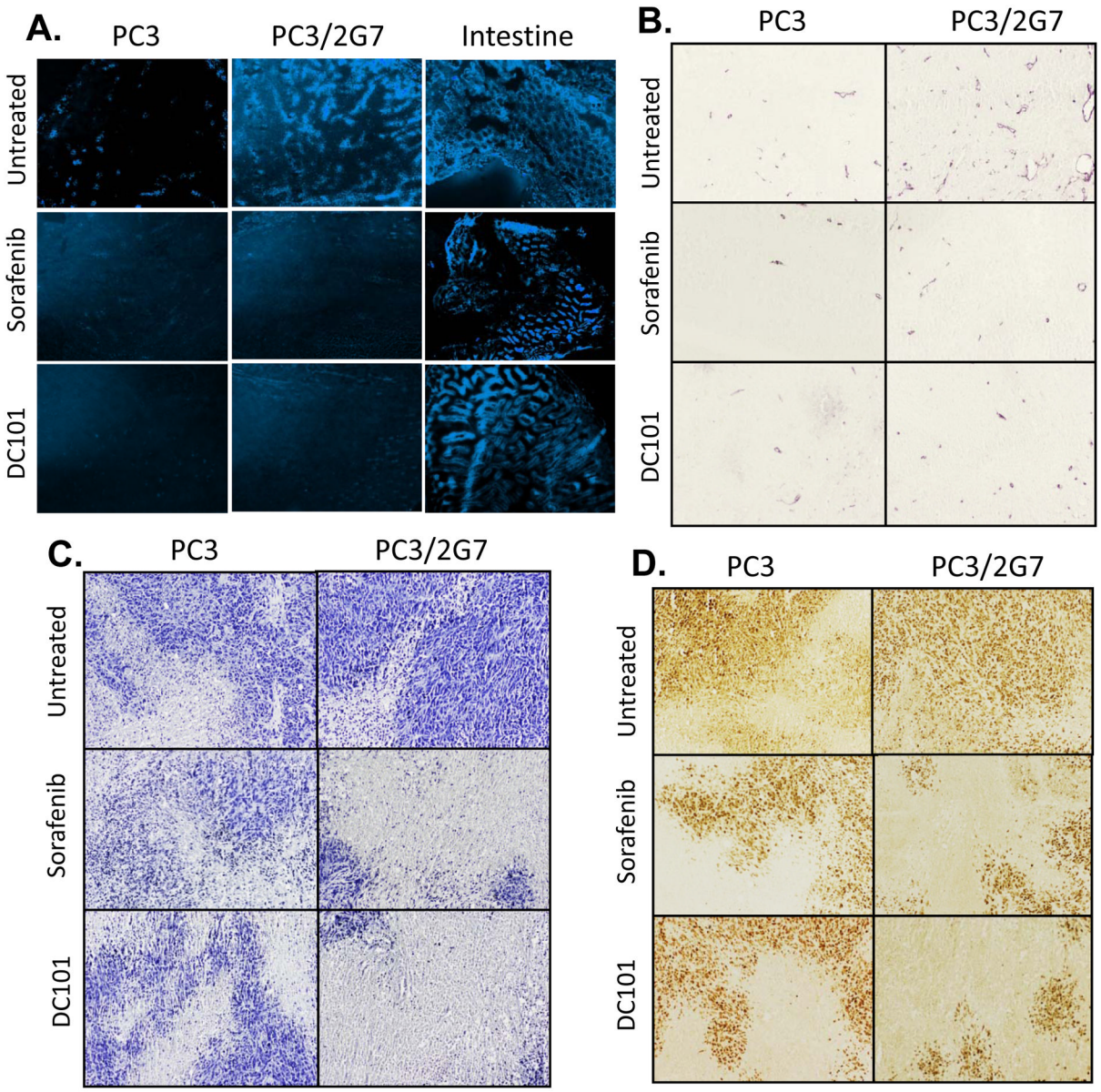

Figure 3. PC3/2G7 tumors are more responsive to sorafenib and DC101 than PC3 tumors

A. Hoechst 33342 staining of drug-free and 21-day sorafinib-treated or 27-day (10 cycle) DC101-treated PC3/2G7 and PC3 tumor cryosections. Mouse intestine from the tumor-bearing mice was used as a normal tissue control. **B**. CD31 stained tumors showing reduction of PC3 and PC3/2G7 tumor microvessel density to a similar low-level following sorafenib or DC101 treatment. **C, D**. Hematoxylin staining of viable tumor regions (C) and PCNA staining of proliferating cells (D) reveals greater decreases in PC3/2G7 tumors compared to PC3 tumors following treatment with sorafenib (21 days) or DC101 (27 days), as in Supplemental Figs. 3 and 4. Shown are representative images of stained cryosections (A) or paraffin-embedded sections (B-D) at 10× magnification.

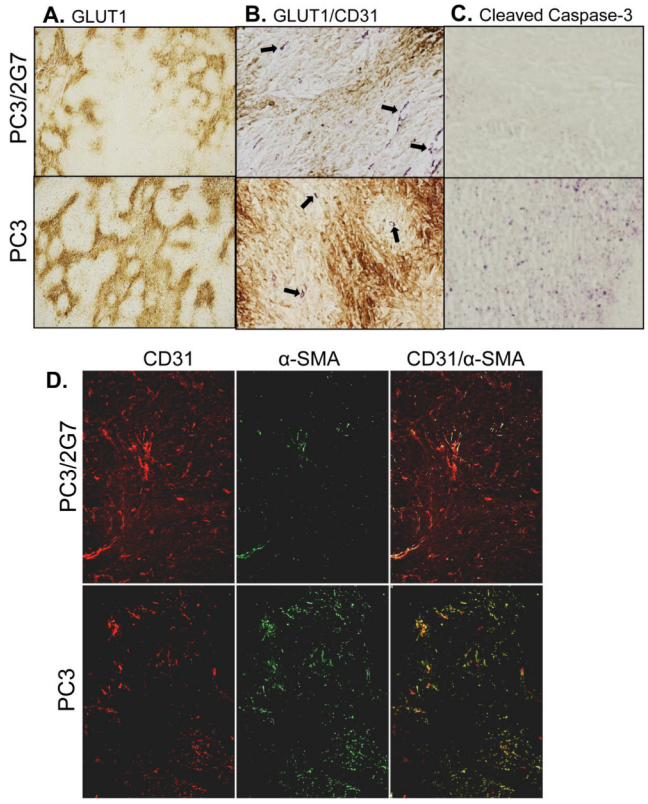

Figure 4. Hypoxia, basal apoptotic status, and pericyte coverage

A. Hypoxia marker GLUT1 staining of PC3/2G7 and PC3 tumors, showing more extensive regions of hypoxia in PC3 tumors. **B**. Double immunostaining of tumor hypoxia (GLUT1 staining, *brown*) and tumor microvessels (CD31, *purple*). Hypoxic regions (*brown staining*) are distant from tumor microvessels (*arrows*). **C**. Immunostaining for cleaved caspase-3, showing significantly fewer basal apoptotic regions in PC3/2G7 compared to PC3 tumors. Shown are representative paraffin-embedded sections at 20×. **D**. Immunofluorescence double-staining of endothelial cells (CD31, *red*) and pericytes (α-SMA, *green*) in PC3/2G7 and PC3 tumor cryosections. The two-color overlay (*right*) visualizes pericyte-covered vascular endothelial cells in yellow. Analysis was performed using an Olympus FSX100 Bio Imaging Navigator fluorescence microscope system. PC3/2G7 tumors show significantly lower pericyte coverage of endothelial cells than PC3 tumors (magnification, 4.2×).

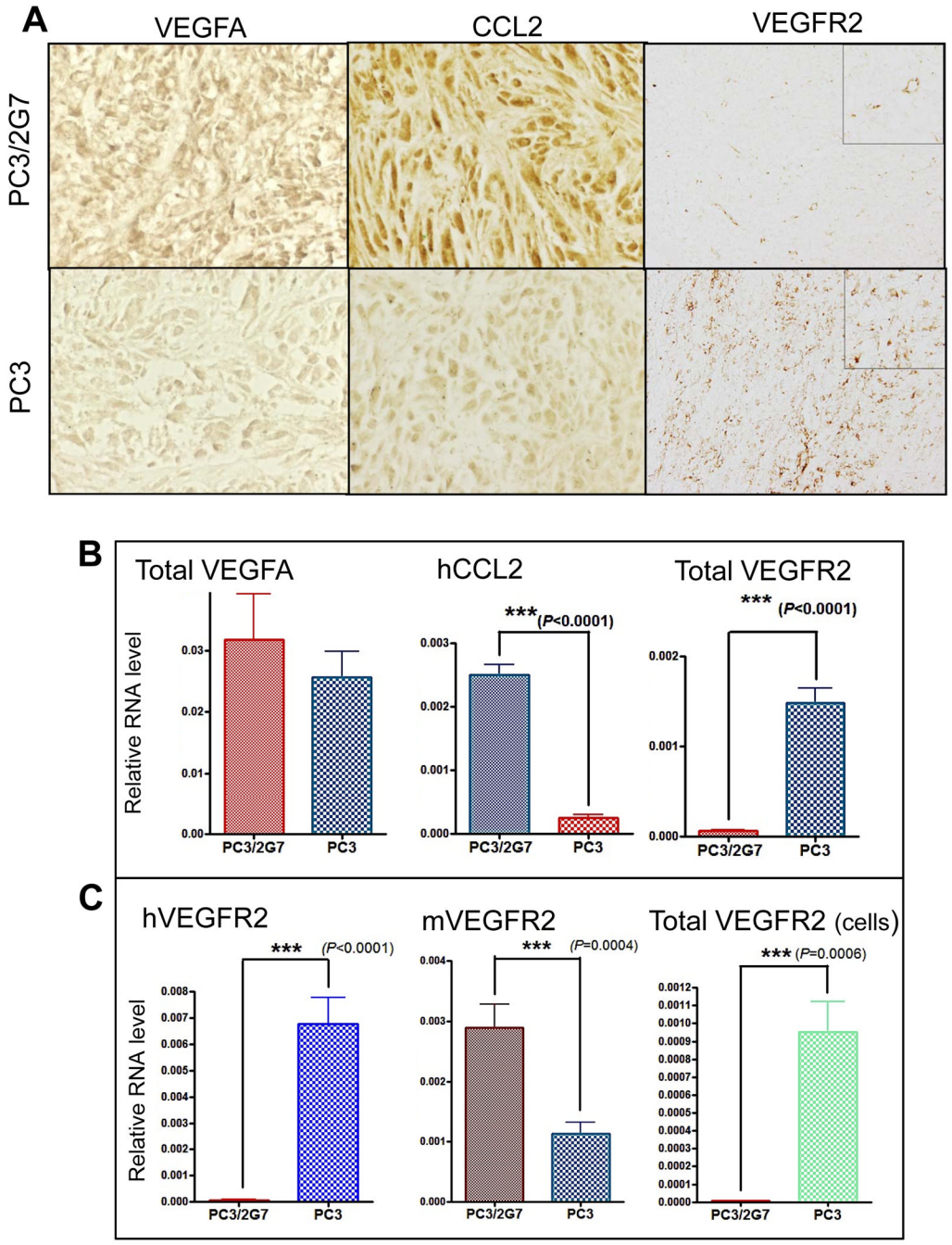

Figure 5. Expression of angiogenic factors by PC3/2G7 and PC3 tumors

A. Representative images showing VEGFA (40×), CCL2 (40×) and VEGFR2 (10×) immunostaining of PC3/2G7 and PC3 tumors. The anti-VEGFR2 antibody recognizes both human and mouse VEGFR2, the anti-CCL2 is a human-specific antibody, and the anti-VEGFA antibody recognizes both human and mouse VEGFA. Images of CCL2 and VEGFA were obtained from paraffin-embedded sections; VEGFR2 images were from cryosections. **B** and **C**, qPCR analysis was carried out for the indicated mouse (m) and human genes (h) using species-specific primers and RNA isolated from n=10 PC3/2G7 tumors and n=12 PC3 tumors. 'Total' indicates qPCR primers did not distinguish mouse from human RNAs. **B**.

VEGFA, VEGFR2 and CCL2 RNA levels. VEGFR2 RNA was significantly down regulated in PC3/2G7 tumors compared to PC3 tumors ($p<0.0001$, ***, two-tailed student's test); CCL2 was significantly increased in PC3/2G7 compared to PC3 tumors ($p<0.0001$, ***, two-tailed student's test). **C**. VEGFR2 RNA assayed using primers specific for human VEGFR2 and mouse VEGFR2, respectively, and also primers recognizing both mouse and human VEGFR2 (total VEGFR2). PC3 tumor cells expressed dramatically higher level of human (i.e., tumor cell-associated) VEGFR2 compared to PC3/2G7 tumor cells.

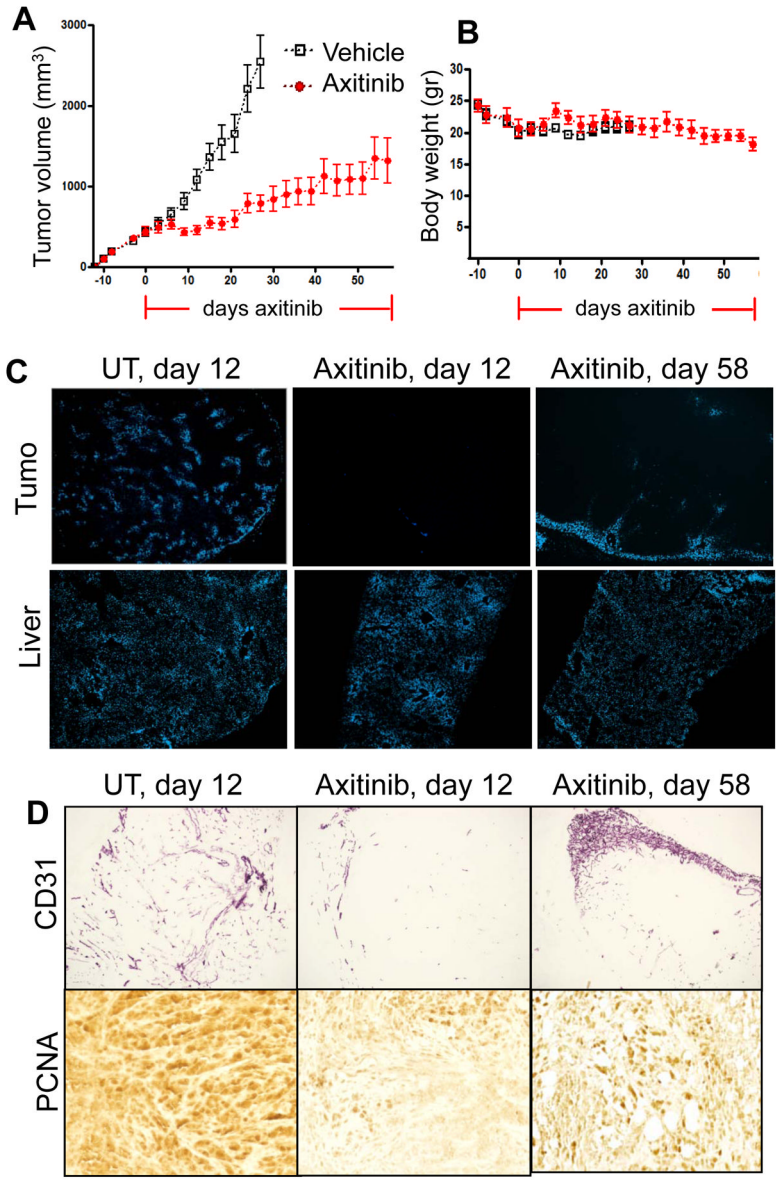

Figure 6. Response of PC3/2G7 tumors to long-term axitinib treatment

A. Change in mean tumor volume for daily axitinib-treated tumors over a 58-day period, with tumor re-growth resuming after day 20. **B**. Body weight measurements in mice bearing PC3/2G7 xenografts. Horizontal red lines along X-axis mark the axitinib treatment period. **C.** Change in functional blood vessels assayed by Hoechst 33342 perfusion in PC3/2G7 tumors analyzed after 12 or 58 days axitinib treatment (magnification, × 4.2). **D**. Changes in microvessel density (CD31 staining; magnification, 4.2×) and cell proliferation (PCNA staining; magnification, 20×) in PC3/2G7 tumors after 58 days axitinib treatment. Increased neovascularization near the tumor periphery and increased tumor cell proliferation were apparent at day 58. See Supplemental Fig. 8 for additional images of neovascularization after 58 days axitinib treatment.

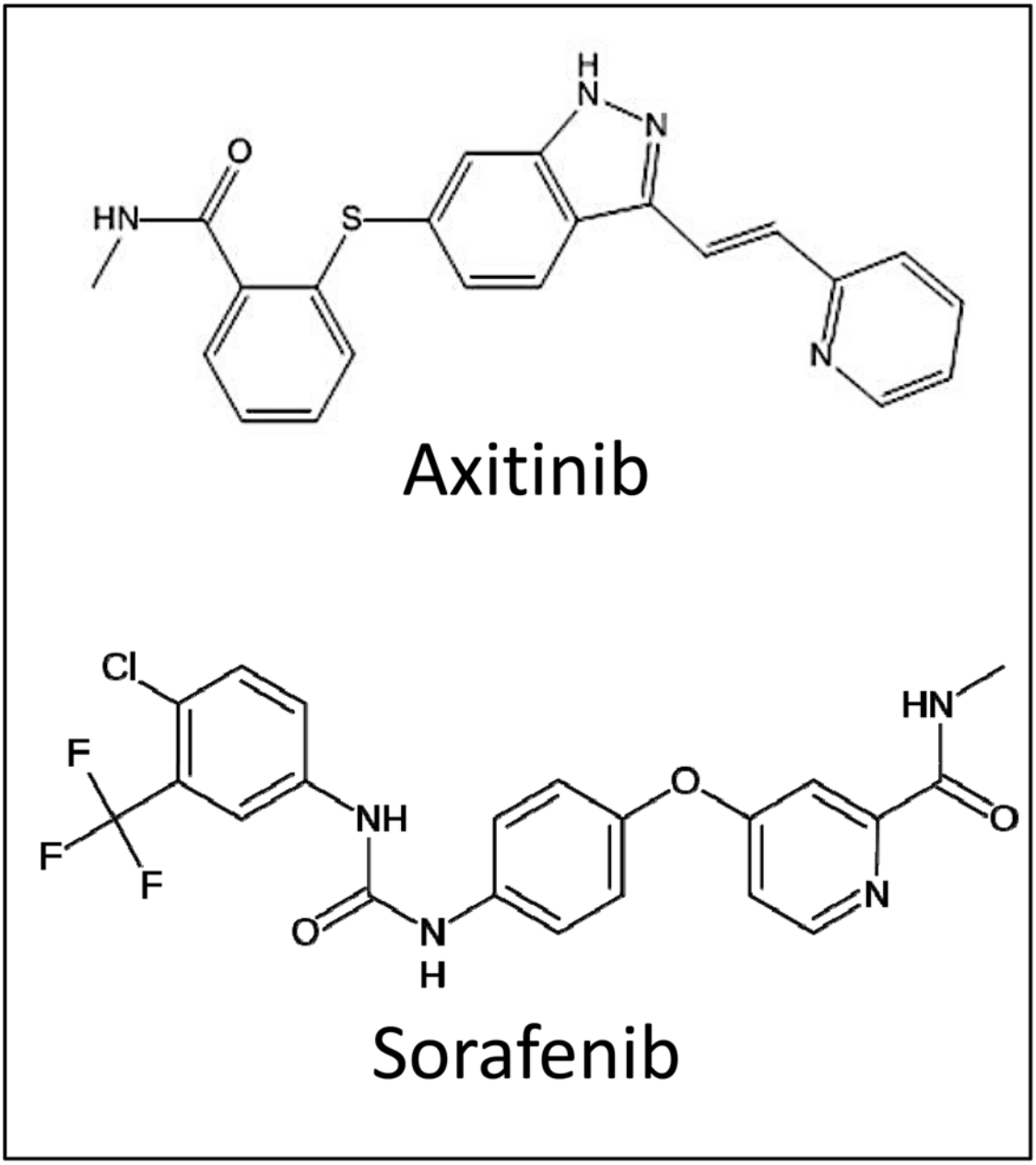

Figure 7.
Chemical structures of axitinib and sorafenib